INSTITUTE OF PHYSICS PUBLISHING JOURNAL OF PHYSICS G: NUCLEAR AND PARTICLE PHYSICS

J. Phys. G: Nucl. Part. Phys. **31** (2005) 825–844 doi:10.1088/0954-3899/31/7/024

# Unified consideration of deep inelastic, quasi-fission and fusion–fission phenomena

**Valery Zagrebaev**[1] **and Walter Greiner**[2]

[1] Flerov Laboratory of Nuclear Reaction, JINR, Dubna, Moscow Region, Russia
[2] Frankfurt Institute for Advanced Studies, J W Goethe-Universität, Frankfurt, Germany

E-mail: valeri.zagrebaev@jinr.ru

Received 27 April 2005
Published 10 June 2005
Online at stacks.iop.org/JPhysG/31/825

**Abstract**

A new approach is proposed for a unified description of strongly coupled deep inelastic (DI) scattering, fusion, fission and quasi-fission (QF) processes of heavy-ion collisions. The standard (most important) degrees of freedom of the nuclear system, unified driving potential, and a unified set of dynamic equations of motion are used in this approach. This makes it possible to perform a full (continuous) time analysis of the evolution of heavy nuclear systems, starting from the approaching stage, moving up to the formation of the compound nucleus and eventually emerging into two final fission fragments. The calculated mass, charge, energy and angular distributions of the reaction products agree well with the corresponding experimental data. It gives us hope to obtain rather accurate predictions for the probabilities of superheavy element formation in near-barrier fusion reactions.

Communicated by Professor H Stöcker

## 1. Introduction

The interest in the synthesis of superheavy nuclei has grown lately due to new experimental results [1] demonstrating the possibility of producing and investigating the nuclei in the region of the so-called 'island of stability'. It is the first (nearest) island of stability. There may be more distant ones [2] The analysis of near-barrier nucleus–nucleus collisions shows that deep inelastic (DI) scattering [3] and quasi-fission (QF) [4–6] are the main reaction channels here, whereas the fusion probability (formation of compound nucleus (CN)) is extremely small. It is the QF process that inhibits fusion by several orders of magnitude. At incident energies around the Coulomb barrier in the entrance channel the fusion probability is about $10^{-2}$ for mass asymmetric reactions induced by $^{48}$Ca and much less for more symmetric combinations used in the 'cold synthesis' (figure 1).

  

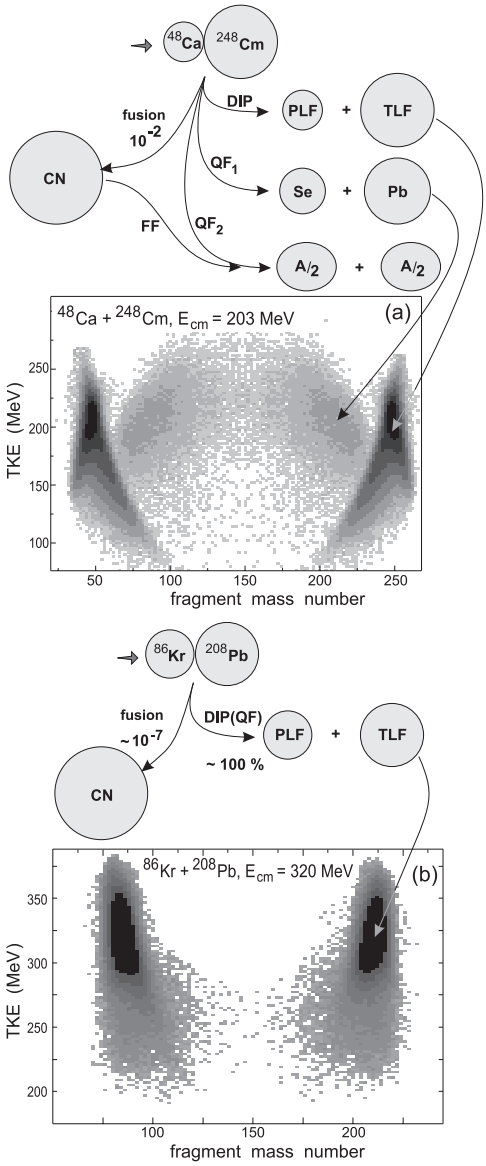


**Figure 1.** Schematic picture of the main reaction channels and two-dimensional experimental TKE-mass plots [5] for $^{48}$Ca+$^{248}$Cm and $^{86}$Kr+$^{208}$Pb near-barrier collisions.

To estimate such a small quantity, first of all, one needs to be able to describe well the main reaction channels, namely DI and QF. The quasi-fission processes are very often indistinguishable from the DI scattering and from regular fission, which is the main decay channel of excited heavy CN. Therefore one needs simultaneous description of all these strongly coupled processes: DI scattering, QF, fusion and regular fission. Note that QF phenomena are revealed in, and could be important also for comparatively light fusing systems [6, 7].

Nucleon exchange and mass transfer play an important role in these reactions, and the mass asymmetry is one of the key degrees of freedom. We will succeed in deriving a set of coupled transport equations for the distance between nuclear centres, dynamic surface deformations, rotations of deformed nuclei, and the variable describing mass distribution between the two fragments. The approaching stage and the scission of the nuclei are most difficult to describe, because the mass transfer cannot be reduced here to a simple change of the mass asymmetry variable. The semi-empirical approach [8] was used for describing the mass transfer at these reaction stages. Starting from the master equation (natural for describing nucleon transfer) we reduce it to the equivalent Langevin equation, which is included in a unified set of the Langevin equations for all the principal degrees of freedom. Thus, for the first time, it becomes possible to describe equally and simultaneously (continuously in time) the whole evolution of low-energy nucleus–nucleus collision at strong channel coupling of DI scattering, QF, fusion (CN formation) and regular fission.

Mass, charge, energy and angular distributions of the reaction products will be calculated and compared with experimental data for $^{136}$Xe+$^{209}$Bi at $E_{\mathrm{c.m.}} = 568$ and 861 MeV [9, 10], $^{86}$Kr+$^{166}$Er at $E_{\mathrm{c.m.}} = 464$ MeV [11] and $^{48}$Ca+$^{248}$Cm at $E_{\mathrm{c.m.}} = 203$ MeV [5]. Detailed time analysis of the reaction dynamics will also be performed in all cases.

## 2. Theoretical model

### *2.1. Potential energy surface*

The proper choice of the unified degrees of freedom playing the most principal role both at approaching stage and at the stage of fission (quasi-fission) is essential and rather difficult. The number of the degrees of freedom should not be too large so that one is able to solve numerically the corresponding set of dynamic equations. On the other hand, however, with a restricted number of collective variables it is difficult to describe simultaneously the DI collision of two separated nuclei and fission or QF of the highly deformed mono-nucleus. The distance between the nuclear centres (corresponding to the elongation of a mono-nucleus), dynamic surface deformations, mutual orientations of deformed nuclei and mass asymmetry are probably the relevant degrees of freedom in fusion–fission dynamics. A schematic view of the considered processes in the space of elongation ($R$), quadrupole deformation ($\beta$) and mass asymmetry ($\alpha = (A_1 - A_2)/(A_1 + A_2)$) is shown in figure 2.

The interaction potential of separated nuclei is calculated rather easily within the folding procedure with effective nucleon–nucleon interaction or parametrized, e.g., by the proximity potential [12]. Of course, some uncertainty remains here, but the height of the Coulomb barrier obtained in these models coincides with the empirical Bass parametrization [13] within 2 to 3 MeV. Dynamic deformations of colliding spherical nuclei and mutual orientation of statically deformed nuclei significantly affect their interaction changing the height of the Coulomb barrier for more than 10 MeV (figure 3). It is caused mainly by a strong dependence of the distance between nuclear surfaces on the deformations and the orientations of nuclei. However, geometrical effects due to a change in the curvature of deformed nuclear surfaces are also important here [14, 15] and should be taken into account in the calculation of the nucleus–nucleus potential. An explicit formula for the geometrical factor for the interaction of deformed and rotated nuclei along with its simple parametrization (free from the unphysical singularity at zero curvature of flat surface) has been proposed in [15].

After contact, the mechanism of interaction of two colliding nuclei becomes more complicated. For fast collisions the nucleus–nucleus potential, $V_{\mathrm{diab}}$, should reveal a strong repulsion at short distances protecting the 'frozen' nuclei from penetrating each other and

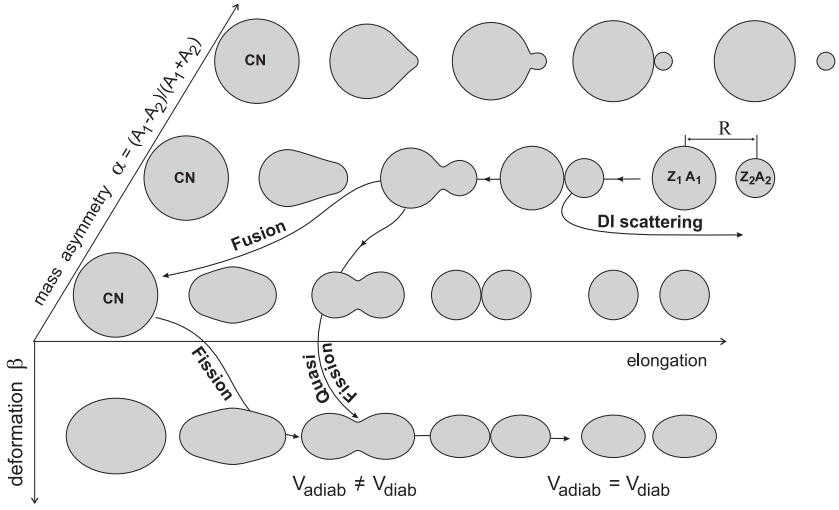


**Figure 2.** Evolution of nuclear system in the variables 'elongation' $R$, 'deformation' $\beta$ and 'mass asymmetry' $\alpha = (A_1 - A_2)/(A_1 + A_2)$.

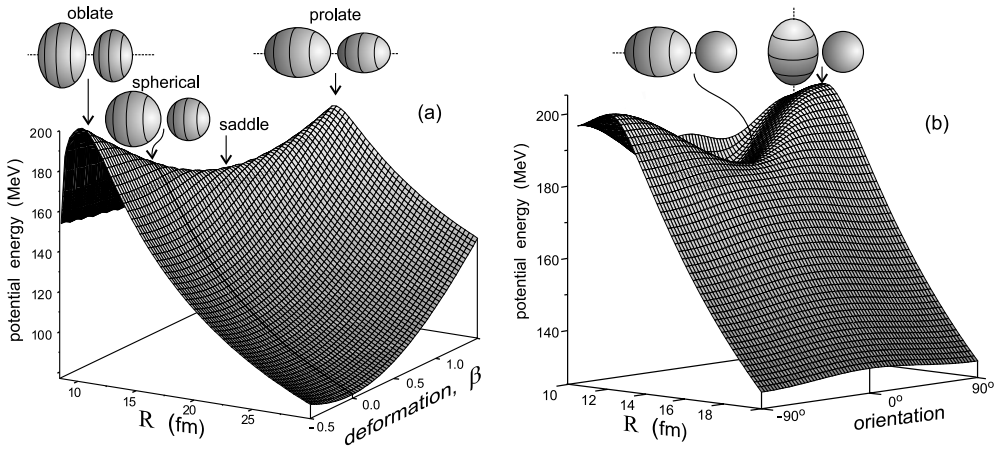


**Figure 3.** (a) Potential energy of $^{48}$Ca+$^{208}$Pb depending on distance and quadrupole dynamic deformations of both nuclei. (b) Potential energy of $^{48}$Ca+$^{238}$U depending on orientation of statically deformed $^{238}$U nucleus ($\beta_2^{gs} = 0.22$).

forming a nuclear matter with double density (diabatic conditions, sudden potential [16]). For slow (near-barrier energies) collisions, when nucleons have enough time to reach equilibrium distribution (adiabatic conditions), the nucleus–nucleus potential energy, $V_{adiab}$, is quite different (figure 4). It is clear that for separated nuclei these potentials coincide.

The calculation of the multi-dimensional adiabatic potential energy surface for heavy nuclear system is a very complicated physical problem, which is not yet fully solved. The two-centre shell model [17] seems to be most appropriate to perform such calculations. However, the simplest version of this model with restricted number of collective coordinates, using overlapping oscillator potentials for the calculation of the single-particle states and resulting shell correction, does not reproduce correct values of the nucleus–nucleus interaction for well-

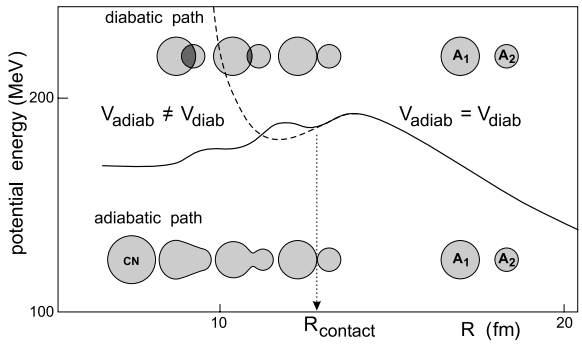


**Figure 4.** Potential energy for $^{48}$Ca+$^{248}$Cm for diabatic (dashed curve) and adiabatic (solid curve) conditions (ground-state deformations of the fragments).

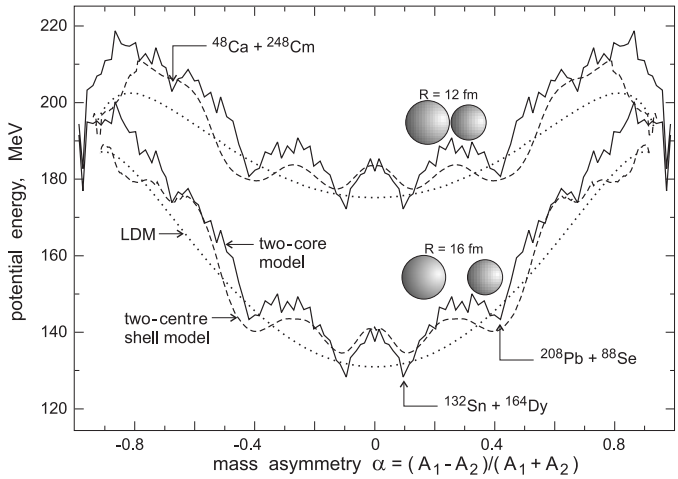


**Figure 5.** Fusion–fission driving potential as a function of mass asymmetry calculated at two fixed distances between nuclei (zero deformations): in the vicinity of the Coulomb barrier, $R = 12$ fm, and for well-separated nuclei, $R = 16$ fm. Dotted, dashed and solid curves correspond to the calculations within the LDM, two-centre shell model and empirical two-core model [18, 19], respectively.

separated nuclei and nuclei at contact point (depending on mass asymmetry). The same holds for the value of the Coulomb barrier and the height of the fission barrier at small deformations. No doubt, within an extended version of this model all these shortcomings may be overcome. We are currently working along this line.

Here we calculated the adiabatic potential energy of the nuclear system within the semi-empirical two-core model of nucleon collectivization [18, 19] based on the two-centre shell model idea [17]. In figure 5 the driving potentials calculated within the two-centre shell model (version of [20]) and within the two-core model are compared for the nuclear system formed in the collision of $^{48}$Ca+$^{248}$Cm leading to a compound nucleus $^{296}$116. As can be seen, the results of two calculations are rather close. At the same time, there are several advantages of the proposed approach. To get a reasonable value for the fission barrier we used the shell corrections at zero and ground state deformations calculated according to [21] and the parametrization of the liquid drop energy proposed in [22]. Based on these values the

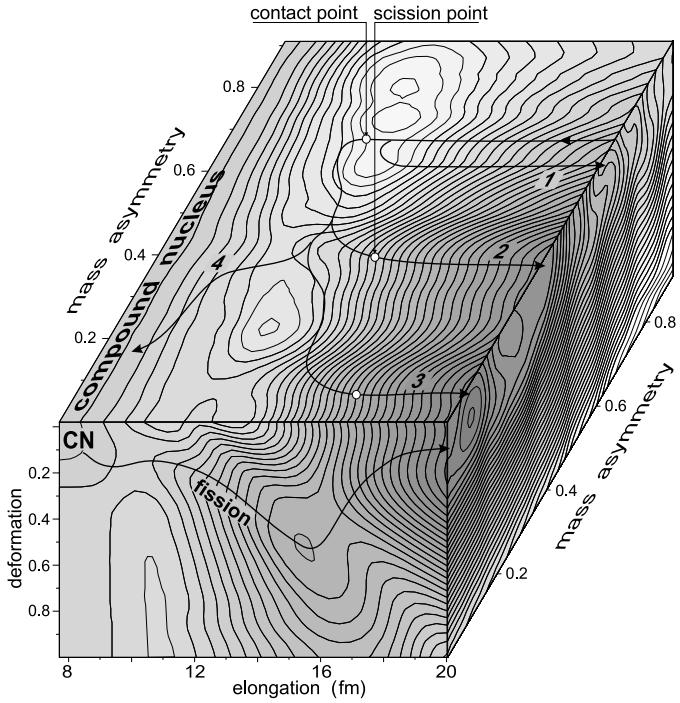


**Figure 6.** Driving potential for the nuclear system formed in $^{48}$Ca+$^{248}$Cm collision. The solid lines show projections of DI (1), QF (2, 3) and CN formation (4) trajectories onto the plane where the deformations of the fragments $\beta = 0$. Also shown is the projection of the regular fission path onto the plane of zero mass asymmetry ($\alpha = 0$). See the correspondence with figure 2 to imagine the shapes.

adiabatic potential was calculated for small deformations. Then it was joined together with the potential of two touching nuclei as it was proposed in [18, 19]. Experimental binding energies of two cores were used, thus giving us the 'true' values of the shell corrections. As a result, the two-core model gives automatically an explicit (experimental) value of the nucleus–nucleus interaction energy in the asymptotic region for well-separated nuclei where it is known (the Coulomb interaction plus nuclear masses). It also gives quite realistic heights of the Coulomb barriers, which is very important for the description of near-barrier heavy-ion reactions. Note that the proposed driving potential is defined in the whole region $R_{\rm CN} < R < \infty$; it is a continuous function at $R = R_{\rm contact}$ and, thus, may be used for a simultaneous description of the whole fusion–fission process.

The resulting multi-dimensional adiabatic potential for $^{296}$116 nuclear system (formed in the reaction $^{48}$Ca+$^{248}$Cm) is shown in figures 6 and 7. The shell effects become apparent in the deep valleys ('cold valleys'), which are distinctly visible in the driving potential. They correspond to the formation of doubly magic nuclei in the exit channel: $^{208}$Pb (at $\alpha \approx 0.4$) and $^{132}$Sn (at $\alpha \approx 0.1$). The two-core shell effects remain important also for strongly overlapping nuclei leading to intermediate deep minima in the potential energy surface. These minima correspond to the shape isomeric states having a two-cluster character with magic or semi-magic cores [23].

The solid curves with arrows in figure 6 show the projections of the trajectories leading to DI (1), QF (2,3) and fusion (4) reaction channels on the plane where the deformations of

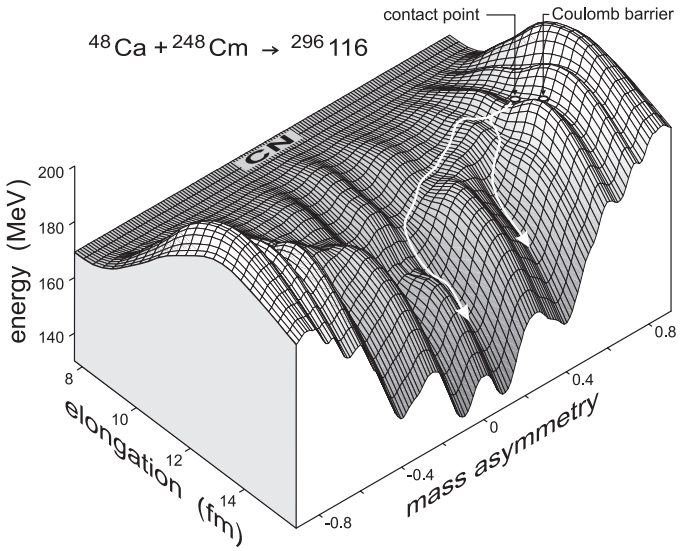


**Figure 7.** Three-dimensional view of the driving potential for $^{48}$Ca+$^{248}$Cm at deformation $\beta = 0.1$. Two white curves with arrows show possible QF paths (2 and 3 in figure 6).

the fragments are zero ($\beta = 0$). Also the projection of the regular fission path on the plane $\alpha = 0$ is shown. Real trajectories are located inside the cubic volume shown in figure 6 at $\beta \neq 0$ and $\alpha \geqslant 0$.

For the nucleus–nucleus collisions at energies well above the Coulomb barrier (e.g., $^{86}$Kr+$^{166}$Er at $E_{\text{c.m.}} = 464$ MeV considered below) we used a simple relaxation scheme, in which after contact a diabatic potential energy gradually turns into an adiabatic one: $V = V_{\text{diab}}[1 - f(t)] + V_{\text{adiab}} f(t)$. Here $t$ is the time of interaction and $f(t)$ is a smoothing function with parameter $\tau_{\text{relax}} \sim 10^{-21}$ s (see, e.g., [24]), $f(t = 0) = 0$, $f(t \gg \tau_{\text{relax}}) = 1$. Our calculations show that even at above-barrier energies the evolution time of the heavy nuclear system in the considered channels is much longer than $\tau_{\text{relax}}$ (adiabatic conditions), and the mass and energy distributions depend weekly on this parameter. At low-energy collisions of heavy nuclei a diabatic reaction stage can be completely ignored and only an adiabatic potential energy can be used. The reason is the large nuclear viscosity and strong friction forces in the entrance channel, which damp very fast the relative motion kinetic energy and lead the nuclear system to a subsequent slow evolution along the minima of the multi-dimensional adiabatic potential energy surface (see below).

### *2.2. Equations of motion*

A proper choice of dynamic equations for the considered degrees of freedom is also not so evident. For the coordinates $R, \beta$ various equations can be used, namely, classical Newtonian, Langevin type [25, 26] or quantum Schrödinger coupled differential equations. The corresponding inertia parameters $\mu_R$ and $\mu_\beta$ can be calculated, for example, within the Werner–Wheeler approach [27] or within the cranking model [28]. But the mass asymmetry $\alpha$ is a discrete variable by its nature. Moreover, the corresponding inertia parameter $\mu_\alpha$ being calculated within the Werner–Wheeler approach becomes infinite at contact (scission) point and for separated nuclei. Thus the nucleon transfer and a change of mass asymmetry require a separate consideration.

The master equation for the distribution function $\varphi(A, t)$

$$\frac{\partial \varphi}{\partial t} = \sum_{A'=A\pm 1} \lambda(A' \to A)\varphi(A', t) - \lambda(A \to A')\varphi(A, t) \tag{1}$$

seems to be good for the description of nucleon transfer in DI scattering [29, 30]. Here $A$ is the number of nucleons in one of the fragments at time $t$ and $\lambda(A' \to A)$ is the macroscopic transition probability. This equation was successfully used for the description of CN formation in strong competition with the dominant QF channels in reactions leading to the synthesis of superheavy nuclei [18, 19].

Equation (1) defines the evolution of the distribution function $\varphi(A, t) \sim \varphi(\alpha, t)$ (not of the variable $\alpha$ itself!), and it cannot be used directly in a common set of coupled differential equations for the coordinates $R$ and $\beta$. However, by certain rules [33, 34] this equation may be transformed first to the Fokker–Planck equation $\frac{\partial \varphi}{\partial t} = -\frac{\partial}{\partial A}(D^{(1)}\varphi) + \frac{\partial^2}{\partial A^2}(D^{(2)}\varphi)$ and then to the Langevin equation $\frac{\mathrm{d}A}{\mathrm{d}t} = D^{(1)} + \sqrt{D^{(2)}}\Gamma(t)$, or (using $\alpha = (2A - A_{\mathrm{CN}})/A_{\mathrm{CN}}$)

$$\frac{\mathrm{d}\alpha}{\mathrm{d}t} = \frac{2}{A_{\mathrm{CN}}} D_A^{(1)}(\alpha) + \frac{2}{A_{\mathrm{CN}}}\sqrt{D_A^{(2)}(\alpha)}\Gamma(t), \tag{2}$$

where $\Gamma(t)$ is the normalized random variable with Gaussian distribution, $\langle \Gamma(t) \rangle = 0$, $\langle \Gamma(t)\Gamma(t') \rangle = 2\delta(t - t')$, and the transport coefficients $D^{(1)}$ and $D^{(2)}$ are defined as follows

$$\begin{aligned} D^{(1)} &= \int (A' - A)\lambda(A \to A')\,\mathrm{d}A', \\ D^{(2)} &= \frac{1}{2}\int (A' - A)^2\lambda(A \to A')\,\mathrm{d}A'. \end{aligned} \tag{3}$$

Note that equation (2) describes an inertialess change of the mass asymmetry $\alpha$, i.e., there is no kinetic energy connected with nucleon transfer. Formally, it is equivalent to the overdamped regime of motion along the mass asymmetry coordinate.

Assuming that sequential nucleon transfers play a main role in mass rearrangement, i.e. $A' = A \pm 1$, we have

$$\begin{aligned} D^{(1)} &= \lambda(A \to A + 1) - \lambda(A \to A - 1), \\ D^{(2)} &= \tfrac{1}{2}\lambda(A \to A + 1) + \lambda(A \to A - 1). \end{aligned} \tag{4}$$

For nuclei in contact the transition probability $\lambda(A' = A \pm 1)$ is defined by nuclear level density [29, 30] $\lambda^{(\pm)} = \lambda_0\sqrt{\rho(A \pm 1)/\rho(A)} \approx \lambda_0 \exp\left(\frac{V(R,\beta,A\pm1) - V(R,\beta,A)}{2T}\right)$. Here $T = \sqrt{E^*/a}$ is the local nuclear temperature, $E^*$ is the excitation energy, $a$ is the level density parameter, and $\lambda_0$ is the nucleon transfer rate ($\sim 10^{22}$ s$^{-1}$ [29, 30]), which may, in principle, depend on excitation energy (the same holds for the diffuseness coefficient $D^{(2)}$). This feature, however, is not completely clear. In [29] the mass diffusion coefficient was assumed to be independent of excitation energy, whereas the microscopic consideration yields a square root dependance of it on nuclear temperature [31]. A linear dependence of the mass diffusion coefficient on $T$ was also used [32]. Here we treat the nucleon transfer rate $\lambda_0$ as a parameter of the model. Later we hope to derive the temperature dependence of this parameter from a systematic analysis of the available experimental data.

Nucleon transfer for slightly separated nuclei is also rather probable. This intermediate nucleon exchange plays an important role in sub-barrier fusion processes [8] and has to be taken into account in equation (2). It can be done by using the following expression for the transition probability

$$\lambda^{(\pm)} = \lambda_0\sqrt{\frac{\rho(A \pm 1)}{\rho(A)}}P_{\mathrm{tr}}(R, \beta, A \to A \pm 1). \tag{5}$$

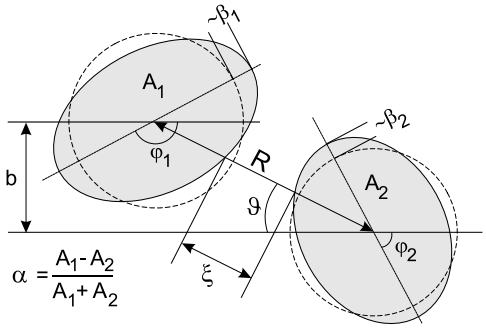


**Figure 8.** Degrees of freedom used in the model.

Here $P_{\rm tr}(R, \beta, A \to A \pm 1)$ is the probability of one nucleon transfer depending on the distance between the nuclear surfaces. This probability goes exponentially to zero at $R \to \infty$ and it is equal to unity for overlapping nuclei. In our calculations, we used the semiclassical approximation for $P_{\rm tr}$ proposed in [8]. Equation (2) along with (5) defines a continuous change of mass asymmetry in the whole space. It is clear that $\frac{{\rm d}\alpha}{{\rm d}t} \to 0$ for far separated nuclei.

Finally, we have the following set of 13 coupled Langevin-type equations for seven degrees of freedom $\{R, \vartheta, \beta_1, \beta_2, \varphi_1, \varphi_2, \alpha\} \equiv \vec{x}$ shown in figure 8:

$$
\begin{aligned}
\frac{{\rm d}R}{{\rm d}t} &= \frac{p_R}{\mu_R} \\
\frac{{\rm d}\vartheta}{{\rm d}t} &= \frac{\hbar\ell}{\mu_R R^2} \\
\frac{{\rm d}\varphi_1}{{\rm d}t} &= \frac{\hbar L_1}{\Im_1} \\
\frac{{\rm d}\varphi_2}{{\rm d}t} &= \frac{\hbar L_2}{\Im_2} \\
\frac{{\rm d}\beta_1}{{\rm d}t} &= \frac{p_{\beta_1}}{\mu_{\beta_1}} \\
\frac{{\rm d}\beta_2}{{\rm d}t} &= \frac{p_{\beta_2}}{\mu_{\beta_2}} \\
\frac{{\rm d}\alpha}{{\rm d}t} &= \frac{2}{A_{\rm CN}} D_A^{(1)}(\alpha) + \frac{2}{A_{\rm CN}}\sqrt{D_A^{(2)}(\alpha)}\Gamma_\alpha(t) \\
\frac{{\rm d}p_R}{{\rm d}t} &= -\frac{\partial V}{\partial R} + \frac{\hbar^2\ell^2}{\mu_R R^3} + \left(\frac{\hbar^2\ell^2}{2\mu_R^2 R^2} + \frac{p_R^2}{2\mu_R^2}\right)\frac{\partial \mu_R}{\partial R} + \frac{p_{\beta_1}^2}{2\mu_{\beta_1}^2}\frac{\partial \mu_{\beta_1}}{\partial R} + \frac{p_{\beta_2}^2}{2\mu_{\beta_2}^2}\frac{\partial \mu_{\beta_2}}{\partial R} \\
&\quad - \gamma_R \frac{p_R}{\mu_R} + \sqrt{\gamma_R T}\Gamma_R(t) \\
\frac{{\rm d}\ell}{{\rm d}t} &= -\frac{1}{\hbar}\frac{\partial V}{\partial \vartheta} - \gamma_{\rm tang}\left(\frac{\ell}{\mu_R R} - \frac{L_1}{\Im_1}a_1 - \frac{L_2}{\Im_2}a_2\right)R + \frac{R}{\hbar}\sqrt{\gamma_{\rm tang} T}\Gamma_{\rm tang}(t) \\
\frac{{\rm d}L_1}{{\rm d}t} &= -\frac{1}{\hbar}\frac{\partial V}{\partial \varphi_1} + \gamma_{\rm tang}\left(\frac{\ell}{\mu_R R} - \frac{L_1}{\Im_1}a_1 - \frac{L_2}{\Im_2}a_2\right)a_1 - \frac{a_1}{\hbar}\sqrt{\gamma_{\rm tang} T}\Gamma_{\rm tang}(t) \\
\frac{{\rm d}L_2}{{\rm d}t} &= -\frac{1}{\hbar}\frac{\partial V}{\partial \varphi_2} + \gamma_{\rm tang}\left(\frac{\ell}{\mu_R R} - \frac{L_1}{\Im_1}a_1 - \frac{L_2}{\Im_2}a_2\right)a_2 - \frac{a_2}{\hbar}\sqrt{\gamma_{\rm tang} T}\Gamma_{\rm tang}(t)
\end{aligned}
\tag{6}
$$

$$\frac{\mathrm{d}p_{\beta_1}}{\mathrm{d}t} = -\frac{\partial V}{\partial \beta_1} + \frac{p_{\beta_1}^2}{2\mu_{\beta_1}^2}\frac{\partial \mu_{\beta_1}}{\partial \beta_1} + \frac{p_{\beta_2}^2}{2\mu_{\beta_2}^2}\frac{\partial \mu_{\beta_2}}{\partial \beta_1} + \frac{\hbar^2 L_1^2}{2\Im_1^2}\frac{\partial \Im_1}{\partial \beta_1} + \left(\frac{\hbar^2 \ell^2}{2\mu_R^2 R^2} + \frac{p_R^2}{2\mu_R^2}\right)\frac{\partial \mu_R}{\partial \beta_1} - \gamma_{\beta_1}\frac{p_{\beta_1}}{\mu_{\beta_1}} + \sqrt{\gamma_{\beta_1} T}\,\Gamma_{\beta_1}(t)$$

$$\frac{\mathrm{d}p_{\beta_2}}{\mathrm{d}t} = -\frac{\partial V}{\partial \beta_2} + \frac{p_{\beta_1}^2}{2\mu_{\beta_1}^2}\frac{\partial \mu_{\beta_1}}{\partial \beta_2} + \frac{p_{\beta_2}^2}{2\mu_{\beta_2}^2}\frac{\partial \mu_{\beta_2}}{\partial \beta_2} + \frac{\hbar^2 L_2^2}{2\Im_2^2}\frac{\partial \Im_2}{\partial \beta_2} + \left(\frac{\hbar^2 \ell^2}{2\mu_R^2 R^2} + \frac{p_R^2}{2\mu_R^2}\right)\frac{\partial \mu_R}{\partial \beta_2} - \gamma_{\beta_2}\frac{p_{\beta_2}}{\mu_{\beta_2}} + \sqrt{\gamma_{\beta_2} T}\,\Gamma_{\beta_2}(t).$$

Here $\varphi_1$ and $\varphi_2$ are the angles of rotation of the nuclei in the reaction plane (their moments of inertia are $\Im_{1,2}(\beta_{1,2}) = k\frac{2}{5}M_{1,2}R_{1,2}^{0\,2}(1+\beta_{1,2}/3)$, $k \approx 0.4$), $a_{1,2} = R/2 \pm (R_1 - R_2)/2$ are the distances from the centres of the fragments up to the middle point between nuclear surfaces, and $R_{1,2} = R_{1,2}^0[1+\sqrt{5/4\pi}\beta_{1,2}P_2(\cos(\varphi_{1,2}-\vartheta))]$ are the nuclear radii. $\gamma_R$, $\gamma_{\mathrm{tang}}$ and $\gamma_{\beta_{1,2}}$ are the friction forces which depend generally on the coordinates $\vec{x}$. For the moment, we ignore the non-diagonal terms of the mass and friction parameters. The so-called 'sliding friction' (which is proportional to the relative velocity of nearest nuclear surfaces $v_{\mathrm{tang}} = \frac{\hbar\ell}{\mu_R R} - \frac{\hbar L_1}{\Im_1}a_1 - \frac{\hbar L_2}{\Im_2}a_2$) is mainly responsible for the dissipation of the angular momentum (see, e.g., [13], p 265 and [35]). In our model, the nucleus–nucleus potential energy depends on the distance between nuclear surfaces $\xi = R - R_{\mathrm{contact}}$, where $R_{\mathrm{contact}} = R_1(\alpha, \beta_1, \varphi_1 - \vartheta) + R_2(\alpha, \beta_2, \varphi_2 - \vartheta)$. Therefore $\frac{\partial V}{\partial \varphi_1} + \frac{\partial V}{\partial \varphi_2} = -\frac{\partial V}{\partial \vartheta}$ and, thus, the total angular momentum $\ell + L_1 + L_2$ is obviously conserved. In asymmetric reactions even if the tangential velocity becomes zero the 'rolling friction' remains due to the difference in angular velocities of two fragments. It changes the angular momenta of the fragments still more up to the formation of the final 'sticking' configuration.

### *2.3. Friction forces and nuclear viscosity*

A number of different mechanisms have been suggested in the literature for being responsible for the energy loss in DI collisions. A discussion on the subject can be found, e.g., in [13, 25, 26, 35]. The uncertainty in the strength of nuclear friction and in its form factor is still large [36]. Because of that and for the sake of simplicity we use here for separated nuclei the phenomenological nuclear friction forces with the Woods–Saxon radial form factor $F(\zeta) = (1+\mathrm{e}^{\zeta})^{-1}$, $\zeta = (\xi - \rho_F)/a_F$. The shift $\rho_F \sim 2$ fm serves to approach the position of the friction shape function to the strong absorption distance which is normally larger than the contact distance $R_{\mathrm{contact}}$ [37]. Thus $\gamma_R^F = \gamma_R^0 F(\xi - \rho_F)$, $\gamma_{\mathrm{tang}}^F = \gamma_t^0 F(\xi - \rho_F)$ and $\gamma_R^0$, $\gamma_t^0$, $\rho_F$ and $a_F \sim 0.6$ fm are the model parameters.

For overlapping nuclei (mono-nucleus configuration) the two-body nuclear friction can be calculated within the Werner–Wheeler approach [27]. The corresponding viscosity coefficient $\mu_0$ is however rather uncertain. From the analysis of fission-fragment kinetic energies it has been estimated to be of the order 1–2 $\times 10^{-23}$ MeV s fm$^{-3}$ [27, 38]. The one-body dissipation mechanism [39, 40] leads in general to stronger nuclear friction and some reduction coefficient for it is often used in specific calculations. Taking into account this uncertainty we use here the Werner–Wheeler approach [27] for calculating the form factors of nuclear friction $\gamma_R^{\mathrm{WW}}(R, \beta_1, \beta_2, \alpha)$ and $\gamma_{\beta_1,\beta_2}^{\mathrm{WW}}(R, \beta_1, \beta_2, \alpha)$ with the viscosity coefficient $\mu_0$ which is treated as a model parameter. To keep the continuity of kinetic energy dissipation at the contact point, where two colliding nuclei form a mono-nucleus, we switched the phenomenological friction $\gamma_R^F$ to $\gamma_R^{\mathrm{WW}}$ by the 'smoothed' (over 0.6 fm) step function $\theta_s(\xi) = (1 - \mathrm{e}^{-\xi/0.3})^{-1}$. The resulting radial friction $\gamma_R = \gamma_R^{\mathrm{WW}}(R, \beta_1, \beta_2, \alpha) + \theta_s(\xi)\gamma_R^F(\xi - \rho_F)$ is shown in

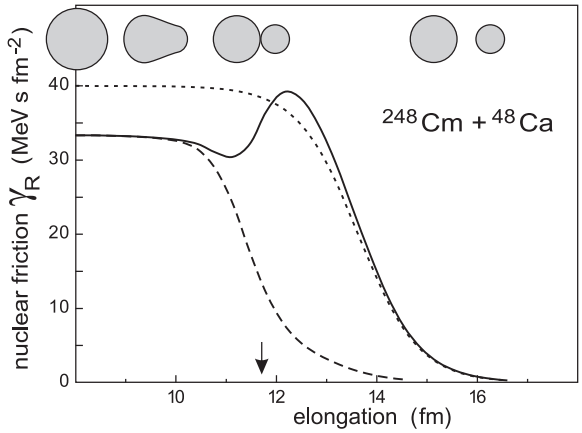


**Figure 9.** The radial nuclear friction for $^{48}$Ca+$^{248}$Cm collision at zero deformations and fixed mass asymmetry $\alpha = 0.675$. Dotted, dashed and solid curves show the phenomenological friction $\gamma_R^F$ in the entrance channel at $\gamma_R^0 = 40 \times 10^{-22}$ MeV s fm$^{-2}$, $\rho_F = 2$ fm and $a_F = 0.6$ fm, the two-body friction $\gamma_R^{\rm WW}$ for mono-nucleus at $\mu_0 = 3 \times 10^{-23}$ MeV s fm$^{-3}$, and the resulting friction, respectively. The contact point is indicated by the arrow.

figure 9. There is no problem with the continuity at the contact point for the nuclear friction $\gamma_{\beta_1,\beta_2}$ associated with the surface deformations.

The two strength parameters of nuclear friction, $\gamma_R^0$ for well-separated nuclei and $\mu_0$ for nuclear viscosity of the deformable mono-nucleus, reflect, on one hand, a possible difference in the mechanisms of dissipation of relative motion kinetic energy in DI collisions of two separated nuclei and nuclear viscosity of a mono-nucleus due to the coupling of collective motion (shape parameters) with the particle–hole excitations. On the other hand, these friction strength parameters are of the same order of magnitude. Using $\mu_0 = 0.2 \times 10^{-22}$ MeV s fm$^{-3}$ proposed in [38] we get the nuclear friction $\gamma_R(\beta = 0) = 4\pi R_0 \mu_0 \approx 15$ MeV s fm$^{-2}$ for a change in the elongation of a spherical nucleus with radius $R_0 = 6$ fm. This value can be compared with the value of nuclear friction of two nuclei in contact $\gamma_R(\xi = 0) = 13$ MeV s fm$^{-2}$ estimated from the 'proximity theorem' [13, p 269]. Nevertheless, as mentioned above, the uncertainty in the values of both parameters is very large [36]. Moreover, microscopic analysis shows that nuclear viscosity may also depend strongly on nuclear temperature [41].

### *2.4. Cross sections*

The cross sections for all the processes were calculated in a natural way: a large number of events (trajectories) were tested for a given impact parameter. Those events in which the nuclear system overcame the fission barrier from the outside and entered the region of small deformations and elongations (see figures 2 and 6), were treated as fusion (CN formation). Subsequent decay of the excited CN was described then within the statistical model with parameters proposed in [42]. The other events correspond to quasi-elastic, DI and QF processes. The double differential cross sections of these processes were calculated as follows:

$$\frac{{\rm d}^2\sigma_\alpha}{{\rm d}\Omega\,{\rm d}E}(E,\theta) = \int_0^\infty b\,{\rm d}b \frac{\Delta N_\alpha(b,E,\theta)}{N_{\rm tot}(b)} \frac{1}{\sin(\theta)\Delta\theta\Delta E}. \tag{7}$$

Here $\Delta N_\alpha(b, E, \theta)$ is the number of events at a given impact parameter $b$ in which the system enters into the channel $\alpha$ (definite mass asymmetry value) with kinetic energy in the region $(E, E + \Delta E)$ and the centre-of-mass outgoing angle in the region $(\theta, \theta + \Delta\theta)$; $N_{\rm tot}(b)$ is the total number of simulated events for a given value of the impact parameter.

Expression (7) describes the mass and energy distributions of the *primary* fragments formed in the reaction. Subsequent de-excitation of these fragments via fission or emission of light particles and gamma rays was taken into account within the statistical model leading to the *final* mass and energy distributions of the reaction fragments. The sharing of the excitation energy between the primary fragments was assumed to be proportional to their masses. Neutron emission during a long evolution of the system going into the QF channels or CN formation was also taken into account. However, it was found that pre-scission and pre-compound neutron evaporation does not influence significantly the gross properties of DI and QF processes (see below).

In our first calculations, we restricted ourselves to the consideration of only one quadrupole dynamic deformation variable $\beta$ instead of independent deformations $\beta_1$ and $\beta_2$ of two fragments. We assumed 'equality of forces', i.e., $C_1\beta_1 = C_2\beta_2$, where $C_{1,2}$ are the LDM stiffness parameters of the fragments [43]. Using this ratio and $\beta_1 + \beta_2 = 2\beta$ the deformations of the fragments were derived from the common variable $\beta$. Removing these simplifications could be rather important. We also ignored the ground state deformations of colliding nuclei. In this case, the potential energy does not depend on the orientation of the nuclei and the nuclear system possesses an axial symmetry, which significantly simplifies the calculation of the adiabatic potential energy surface. The orientation effects in the formation of CN and quasi-fission channels will be considered in our forthcoming publication.

## 3. DI, QF and FF processes

At first we analysed the collision of very heavy nuclei, $^{136}$Xe+$^{209}$Bi at energies $E_{\rm c.m.} =$ 568 MeV and 861 MeV [9, 10], where the DI process should dominate due to expected prevalence of the Coulomb repulsion over nuclear attraction and the impossibility of CN formation. In that case, the reaction mechanism depends mainly on the nucleus–nucleus potential at a contact distance (which determines the grazing angle), on the friction forces at this region (which determine the energy loss) and on the nucleon transfer rate at contact.

For the nucleus–nucleus interaction we used the proximity potential [12] with $r_0 = 1.16$ fm. For separated nuclei we chose the friction forces with $\gamma_R^0 = 40 \times 10^{-22}$ MeV s fm$^{-2}$, $\rho_F = 2$ fm and $a_F = 0.6$ fm and equal tangential and radial friction strengths $\gamma_t^0 = \gamma_R^0$ as it was recommended in [44]. In spite of a short penetration of nuclei into each other, the reaction cross sections were found to be sensitive to the value of nuclear viscosity of the mono-nucleus, $\mu_0$, mainly due to the large dynamic deformations of the reaction fragments. The values of $\mu_0 = 1 \times 10^{-22}$ and $3 \times 10^{-22}$ MeV s fm$^{-3}$ have been used to describe properly the reaction cross sections at the centre-of-mass beam energies of 568 and 861 MeV respectively. These values are larger than those found for low excited fissile nuclei [38]. It evidently indicates a temperature dependence of nuclear viscosity. The nucleon transfer rate was fixed at $\lambda_0 = 0.1 \times 10^{22}$ s$^{-1}$. This rather small value was found to be sufficient to reproduce the mass distributions of reaction products at both energies.

In figure 10 the angular, energy and charge distributions of the Xe-like fragments are shown comparing with our calculations (histograms). In accordance with experimental conditions at the incident energy $E_{\rm c.m.} = 861$ MeV only the events with the energy loss higher than 50 MeV and with the scattering angles in the region of $18^\circ \leqslant \theta_{\rm c.m.} \leqslant 128^\circ$ were accumulated.

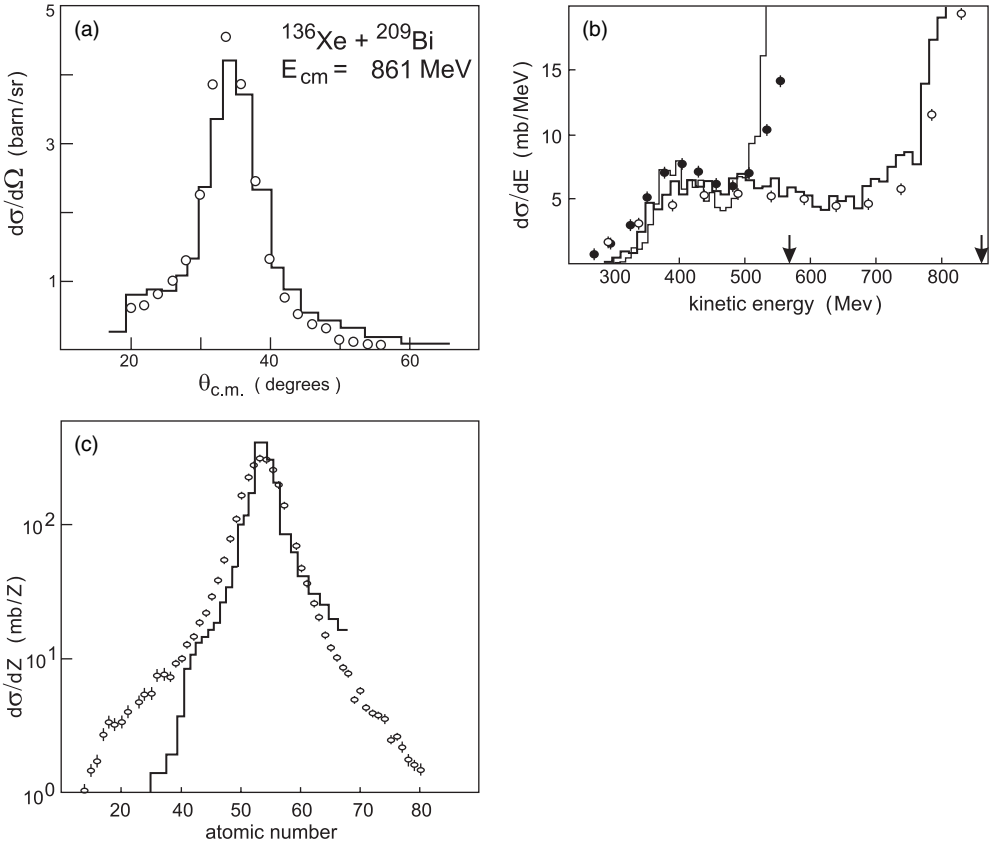


**Figure 10.** Angular (a), energy (b) and charge (c) distributions of the Xe-like fragments obtained in the $^{136}$Xe+$^{209}$Bi reaction at $E_{\text{c.m.}} = 861$ MeV. Experimental data are from [10]. Histograms are the theoretical predictions. The energy distribution is also shown in (b) for $E_{\text{c.m.}} = 568$ MeV [9] (full circles and thin histograms). The arrows in (b) indicate the corresponding beam energies.

The minimal values of kinetic energy of the reaction fragments (∼300 MeV) are almost independent of the beam energies. This indicates that these events correspond to the same re-separation distance and resemble the fission process, though the CN is not formed here. Some underestimation of the low-$Z$ shoulder in figure 10(c) could be due to the contribution of sequential fission of highly excited reaction fragments not accounted for in the present model.

At the second step, we analysed the reaction $^{86}$Kr+$^{166}$Er at $E_{\text{c.m.}} = 464$ MeV [11], in which the nuclear attractive forces may lead, in principle, to the formation of a mono-nucleus and of a CN. The adiabatic potential energy surface, QF and fusion–fission (FF) processes should in this case play a more important role. For the analysis of this reaction, we used the same value of the nucleon transfer rate and the same friction forces as in the previous case. For the nuclear viscosity, we choose the value $\mu_0 = 2 \times 10^{-22}$ MeV s fm$^{-3}$ because of intermediate values of excitation energies available here as compared with the two previous reactions.

The interaction time is one of the most important characteristics of nuclear reactions, though it cannot be measured directly. It depends strongly on the reaction channel. The time distribution of all the $^{86}$Kr+$^{166}$Er collisions at $E_{\text{c.m.}} = 464$ MeV, in which the kinetic energy loss is higher than 35 MeV, is shown in figure 11. The interaction time was calculated

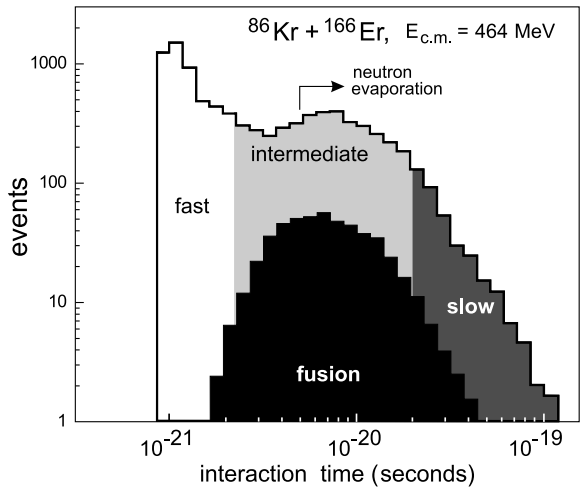


**Figure 11.** Time distribution of all the simulated events for $^{86}$Kr+$^{166}$Er collisions at $E_{\text{c.m.}} = 464$ MeV, in which the energy loss was found higher than 35 MeV (total $10^5$ events). Conditionally, fast ($<2 \times 10^{-21}$ s), intermediate and slow ($>2 \times 10^{-20}$ s) collisions are marked by different shades (white, light grey and dark grey, respectively). The black area corresponds to CN formation (estimated cross section is 120 mb), and the arrow shows the interaction time after which the neutron evaporation may occur.

starting from $t = 0$ at $R = R_{\text{max}} = 40$ fm up to the moment of scission into two fragments ($R > R_{\text{scission}}$, $p_R > 0$) or up to CN formation. The approaching time (path from $R_{\text{max}}$ to $R_{\text{contact}}$) in the entrance channel is very short (4–5 $\times$ $10^{-22}$ s depending on the impact parameter) and may be ignored here. All the events are divided relatively into three groups: fast ($\tau_{\text{int}} < 20 \times 10^{-22}$ s), intermediate and slow ($\tau_{\text{int}} > 200 \times 10^{-22}$ s).

A two-dimensional plot of the energy–mass distribution of the primary fragments formed in the $^{86}$Kr+$^{166}$Er reaction at $E_{\text{c.m.}} = 464$ MeV is shown in figure 12. Inclusive angular, charge and energy distributions of these fragments (with energy losses more than 35 MeV) are shown in figure 13. Rather good agreement with experimental data of all the calculated DI reaction properties can be seen, which was never obtained before in dynamic calculations. Underestimation of the yield of low-$Z$ fragments (figure 13(c)) could again be due to the contribution of sequential fission of highly excited reaction participants not accounted in the model at the moment.

In most of the damped collisions ($E_{\text{loss}} > 35$ MeV) the interaction time is rather short (several units of $10^{-21}$ s). These fast events correspond to grazing collisions with intermediate impact parameters. They are shown by the white areas in figures 11 and 13(b) and by the open circles in the two-dimensional TKE-mass plot (figure 12(b)). Note that a large amount of kinetic energy is dissipated here very fast at relatively low mass transfer (more than 200 MeV during several units of $10^{-21}$ s).

The other events correspond to much slower collisions with large overlap of nuclear surfaces and significant mass rearrangement. In the TKE-mass plot these events spread over a wide region of mass fragments (including symmetric splitting) with kinetic energies very close to the kinetic energy of fission fragments. The solid line in figure 12(b) corresponds to the potential energy at scission point $V(r = R_{\text{scission}}, \beta, \alpha) + Q_{gg}(\alpha)$ minimized over $\beta$. The scission point is calculated here as $R_{\text{scission}}(\alpha, \beta) = (1.4/r_0)[R_1(A_1, \beta_1) + R_2(A_2, \beta_2)] + 1$ fm, $Q_{gg}(\alpha) = B(A_1) + B(A_2) - B(^{86}\text{Kr}) - B(^{166}\text{Er})$ and $B(A)$ is the binding energy of a nucleus

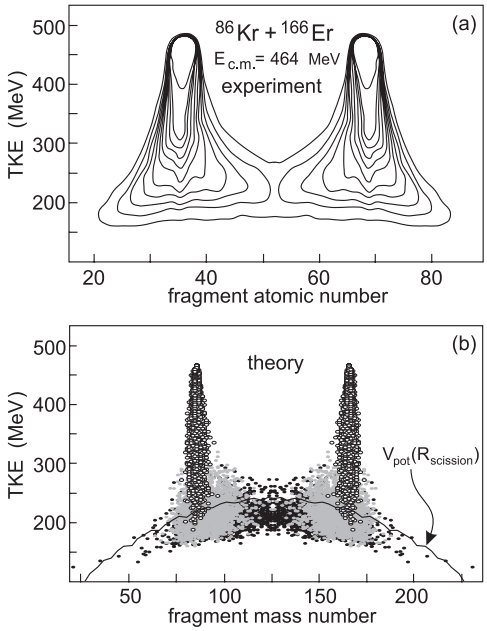


**Figure 12.** (a) TKE-charge distribution of the $^{86}$Kr+$^{166}$Er reaction products at $E_{\text{c.m.}} = 464$ MeV [11]. (b) Calculated TKE-mass distribution of the primary fragments. Open, grey and black circles correspond to the fast ($<2 \times 10^{-21}$ s), intermediate and long ($>2 \times 10^{-20}$ s) events (overlapping each other on the plot).

*A*. Some gap between the two groups in the time and energy distributions can also be seen in figures 11 and 13(b). All these make the second group of slow events quite distinguished from the first one. These events are more similar to fission than to deep inelastic processes. Formally, they can also be marked as quasi-fission.

For the highly excited nuclear system, neutron evaporation is possible before re-separation of the fragments and also on the path to the formation of a CN. In figure 11 the arrow indicates the interaction time after which the probability of neutron emission becomes noticeable in the system $^{86}$Kr+$^{166}$Er at excitation energy of 200 MeV (reached at this moment of interaction time). However, the calculations show that only a few neutrons (less than 2 on average) may evaporate at this intermediate reaction stage and this does not influence significantly the angular, energy and mass distributions of the reaction products. Neutron evaporation from the excited primary fragments dominates in this reaction [45] changing the mass and energy distributions of detected particles.

Let us consider now the near-barrier fusion reaction leading to the formation of a superheavy nucleus in which the QF process plays a dominant role. The competition between CN formation and QF processes in these reactions was already analysed using the master equations (with restricted number of variables) [18, 19] and within the Langevin equations, in which the mass asymmetry coordinate $\alpha$ was treated on the same base as elongation and deformation [46]. In both cases, the calculations started from the contact configuration thereby ignoring the approaching stage and the DI channels. Here we perform a complete analysis of such a reaction.

A typical trajectory of the nuclear system in the collision of $^{48}$Ca+$^{248}$Cm at $E_{\text{c.m.}} =$ 203 MeV (zero impact parameter) is shown in figures 14 and 15. This trajectory leads the

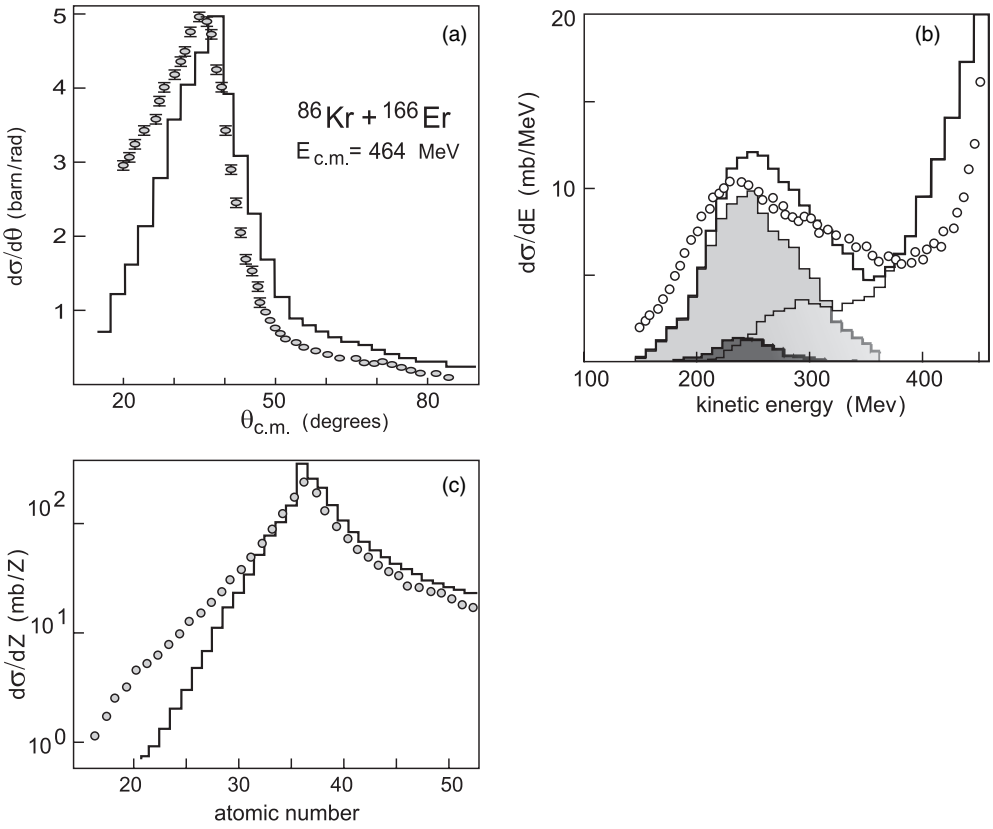


**Figure 13.** Angular (a), energy (b) and charge (c) distributions of the $^{86}$Kr+$^{166}$Er reaction products at $E_{\mathrm{c.m.}} = 464$ MeV. Experimental data (points) are from [11]. Overlapping white, light and dark grey areas in (b) show the contributions of the fast, intermediate and slow events, respectively (see figures 11 and 12(b)).

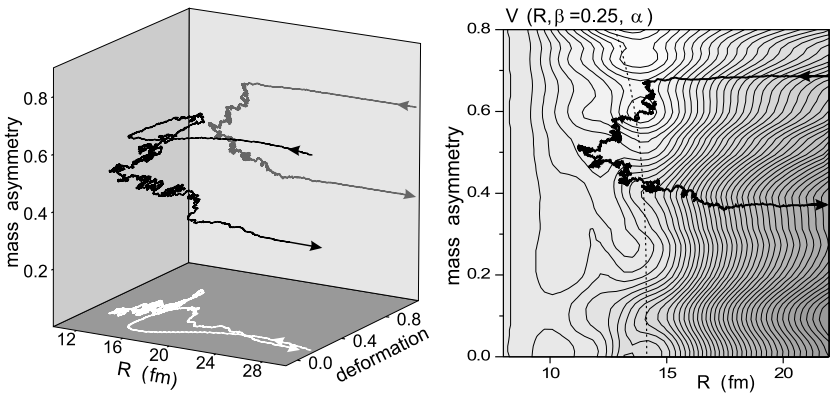


**Figure 14.** One of the trajectories leading to the QF exit channel in the collision of $^{48}$Ca+$^{248}$Cm at $E_{\mathrm{c.m.}} = 203$ MeV. It is drawn in the three-dimensional space of 'elongation–deformation–mass asymmetry' (to the left) and projected onto the plane of deformation $\beta = 0.25$ (to the right).

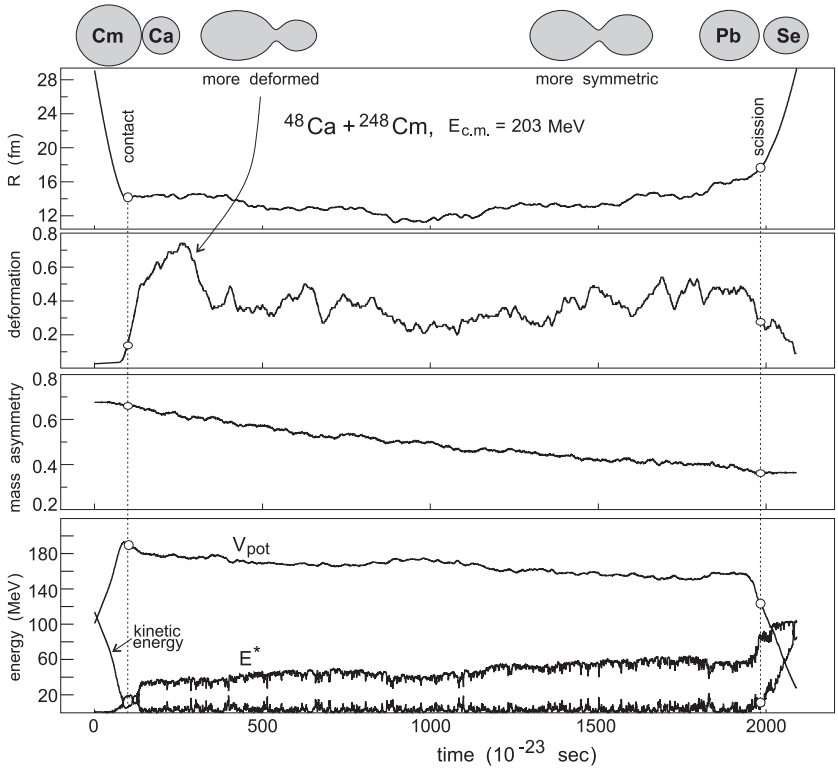


**Figure 15.** Change of elongation, deformation, mass asymmetry, potential, kinetic and excitation energies along the trajectory shown in figure 14.

system to the QF channel. After overcoming the Coulomb barrier the fragments become first very deformed, then the mass asymmetry gradually decreases and the system finds itself in the quasi-fission valley with one of the fragments close to the doubly magic nucleus $^{208}$Pb. After contact, the nuclear system has almost zero kinetic energy up to scission, and the regions with higher potential energy are surmounted mainly due to the fluctuations. The excitation energy of the system (temperature) gradually increases (very sharply on descent stage to the scission point).

Figure 16 shows the calculated correlation of the total kinetic energy and the mass distributions of the reaction products along with inclusive mass distribution for the $^{48}$Ca+$^{248}$Cm reaction at near-barrier energy of $E_{\mathrm{c.m.}} = 203$ MeV. Good agreement with experimental data (compare with figure 1(a)) is rather evident. The tails of DI component to the unphysical high energies (higher than $E_{\mathrm{c.m.}}$ at $A_1 \sim 50$ and $A_2 \sim 250$) and to very low energies with more symmetric mass combinations in figure 1(a) (absent in the theoretical calculations) are the results of specific experimental procedure [47].

The probability for CN formation in this reaction was found to be very small and depended greatly on the incident energy. As was already mentioned, due to the strong dissipation of kinetic energy only the fluctuations (random forces) define the dynamics of the system after the contact of two nuclei. At near-barrier collisions the excitation energy (temperature) of the system is rather low, the fluctuations are weak and the system chooses the most probable path to the exit channel along the quasi-fission valley. However, at non-zero excitation energy

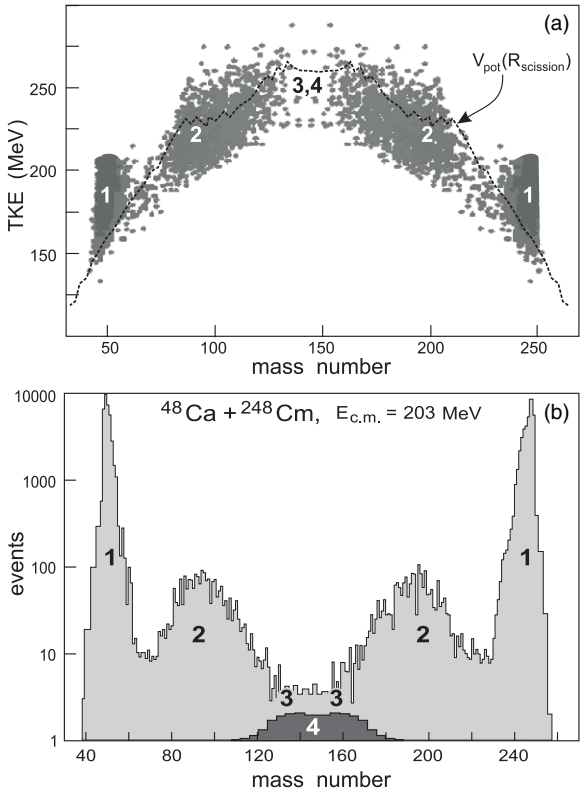


**Figure 16.** (a) Calculated TKE-mass distribution of primary reaction products in the collision of $^{48}$Ca+$^{248}$Cm at $E_{c.m.} = 203$ MeV. (b) Contributions of DI (1), QF (2,3) and fusion–fission (4) processes to inclusive mass distribution (see the corresponding trajectories in figure 6).

there is a chance for the nuclear system to overcome the multi-dimensional inner potential barriers and find itself in the region of CN configuration (small deformation and elongation). Within the Langevin calculations, a great number of events should be tested to find this low probability. For the studied reaction, for example, only several fusion events have been found among more than $10^5$ total tested events (see figure 16(b)). The cross section of CN formation at the beam energy of $E_{c.m.} = 203$ MeV was estimated to be only 0.02 mb in reasonable agreement with those found previously [19] and with the yield of evaporation residues in this reaction [1]. Detailed analysis of CN formation in 'cold' (more symmetric) and 'hot' (asymmetric) fusion reactions leading to the formation of superheavy elements will be done separately.

## 4. Conclusion

For near-barrier collisions of heavy ions, it is very important to perform a combined (unified) analysis of all strongly coupled channels: deep inelastic scattering, quasi-fission, fusion and regular fission. We demonstrate in this paper, for the first time, that this ambitious goal has now become possible. A unified potential energy surface is derived determining the evolution of the nuclear system in all the channels. This potential has also appropriate values of the Coulomb barriers in the entrance channel and proper values of the fission barriers in the exit

one. A unified set of dynamic Langevin-type equations is proposed for the simultaneous description of DI and fusion–fission processes. For the first time, the whole evolution of the heavy nuclear system can be traced starting from the approaching stage and ending in DI, QF and/or fusion–fission channels. Satisfactory agreement of these first calculations with experimental data gives us hope not only to obtain rather accurate predictions of the probabilities for superheavy element formation but also to clarify much better than before the mechanisms of quasi-fission and fusion–fission processes. Also the determination of such fundamental characteristics of nuclear dynamics as the nuclear viscosity and the nucleon transfer rate is now possible. New and more experiments on near-barrier collisions of heavy nuclei with accurate and simultaneous detection of all significant reaction channels are needed.

## Acknowledgments

The authors are indebted to Professors M G Itkis and Yu Ts Oganessian for many fruitful discussions on the problem. The work was supported partially by the DFG-RFBR collaboration project under grant no 04-02-04008.

## References

[1] Oganessian Yu Ts *et al* 2001 *Phys. Rev.* C **63** 011301(R)
Oganessian Yu Ts *et al* 2004 *Phys. Rev.* C **69** 021601(R)
Oganessian Yu Ts *et al* 2004 *Phys. Rev.* C **69** 054607
Oganessian Yu Ts *et al* 2004 *Phys. Rev.* C **70** 064609
[2] Greiner W 2001 *Proc. Int. Conf. on Fusion Dynamics at the Extremes (Dubna)* ed Yu Ts Oganessian and V I Zagrebaev (Singapore: World Scientific) p 1
[3] Volkov V V 1984 *Reactions of Deep-Inelastic Transfer* (Moscow: Energoatomizdat) (in Russian)
[4] Péter J, Ngô C, Plasil F, Tamain B, Berlanger M and Hanappe F 1977 *Nucl. Phys.* A **279** 110
[5] Itkis M G *et al* 2001 *Proc. Int. Conf. on Fusion Dynamics at the Extremes (Dubna)* ed Yu Ts Oganessian and V I Zagrebaev (Singapore: World Scientific) p 93
[6] Itkis M G *et al* 2004 *Nucl. Phys.* A **734** 136
[7] Berriman A, C Hinde D J, Dasgupta M, Morton C R, Butt R D and Newton J O 2001 *Nature* **413** 144
[8] Zagrebaev V I 2003 *Phys. Rev.* C **67** 061601(R)
[9] Wilcke W W, Birkelund J R, Hoover A D, Huizenga J R, Schröder W U, Viola V E Jr, Wolf K L and Mignerey A C 1980 *Phys. Rev.* C **22** 128
[10] Wollersheim H J, Wilcke W W, Birkelund J R, Huizenga J R, Schröder W U, Freiesleben H and Hilscher D 1981 *Phys. Rev.* C **24** 2114
[11] Gobbi A, Lynen U, Olmi A, Rudolf G and Sann H 1981 *Proc. Int. School of Phys. 'Enrico Fermi', Course LXXVII (Varenna, 1979)* (Amsterdam: North-Holland) p 1
[12] Blocki J, Randrup J, Swiatecki W J and Tsang C F 1977 *Ann. Phys., N.Y.* **105** 427
[13] Bass R 1980 *Nuclear Reactions with Heavy Ions* (Berlin: Springer) p 326
[14] Gontchar I I, Dasgupta M, Hinde D J, Butt R D and Mukherjee A 2002 *Phys. Rev.* C **65** 034610
[15] Zagrebaev V I and Samarin V V 2004 *Yad. Fiz.* **67** 1488
Zagrebaev V I and Samarin V V 2004 *Phys. At. Nucl.* **67** 1462 (Engl. Transl.)
[16] Scheid W, Ligensa R and Greiner W 1968 *Phys. Rev. Lett.* **21** 1479
[17] Mosel U, Maruhn J and Greiner W 1971 *Phys. Lett.* B **34** 587
Maruhn J and Greiner W 1972 *Z. Phys.* **251** 431
[18] Zagrebaev V I 2001 *Phys. Rev.* C **64** 034606
[19] Zagrebaev V I 2004 *Tours Symp. on Nucl. Phys. V, AIP Conf. Proc.* **704** 31
[20] Iwamoto A, Yamaji S, Suekane S and Harada K 1976 *Prog. Theor. Phys.* **55** 115
[21] Möller P *et al* 1995 *At. Data Nucl. Data Tables* **59** 185
[22] Myers W D and Swiatecki W 1974 *Ann. Phys., N.Y.* **84** 186
[23] Zagrebaev V I, Itkis M G and Oganessian Yu Ts 2003 *Yad. Fiz.* **66** 1069
Zagrebaev V I, Itkis M G and Oganessian Yu Ts 2003 *Phys. At. Nucl.* **66** 1033 (Engl. transl.)
[24] Bertsch G F 1978 *Z. Phys.* A **289** 103
Cassing W and Nörenberg W 1983 *Nucl. Phys.* A **401** 467

[25] Abe A, Ayik S, Reinhard P-G and Suraud E 1996 *Phys. Rep.* **275** 49
[26] Fröbrich P and Gonchar I I 1998 *Phys. Rep.* **292** 131
[27] Werner F G and Wheeler J A (unpublished)
Davies K T R, Sierk A J and Nix J R 1976 *Phys. Rev.* C **13** 2385
[28] Eisenberg J M and Greiner W 1972 *Microscopic Theory of the Nucleus* (Amsterdam: North-Holland)
[29] Nörenberg W 1974 *Phys. Lett.* B **52** 289
[30] Moretto L G and Sventek J S 1975 *Phys. Lett.* B **58** 26
[31] Ayik S, Schürmann B and Nörenberg W 1976 *Z. Phys.* A **279** 174
[32] Schmidt R and Wolschin G 1980 *Z. Phys.* A **296** 215
[33] Risken H 1984 *The Fokker Planck Equation* (Berlin: Springer)
[34] Gardiner C W 1990 *Stochastic Methods* (Berlin: Springer)
[35] Schröder W U and Huizenga J R 1984 Damped nuclear reactions *Treatise on Heavy-Ion Science* vol 2, ed D A Bromley (New York: Plenum) p 140
[36] Hilscher D and Rossner H 1993 *Proc. Int. School-Seminar on Heavy Ion Physics (Dubna)* ed Yu Ts Oganessian *et al* (Dubna: JINR) p 230
[37] Gross D H E and Kalinowski H 1974 *Phys. Lett.* B **48** 302
[38] Davies K T R, Managan R A, Nix J R and Sierk A J 1977 *Phys. Rev.* C **16** 1890
[39] Randrup J and Swiatecki W J 1984 *Nucl. Phys.* A **429** 105
[40] Feldmeier H 1987 *Rep. Prog. Phys.* **50** 915
[41] Hofmann H 1997 *Phys. Rep.* **284** 137
Ivanyuk F A 2000 *Proc. on Dynamical Aspects of Nuclear Fission (Slovakia, 1998)* ed Yu Ts Oganessian, J Kliman and S Gmuca (Singapore: World Scientific) p 424
[42] Zagrebaev V I, Aritomo Y, Itkis M G, Oganessian Yu Ts and Ohta M 2002 *Phys. Rev.* C **65** 014607
[43] Bohr A and Mottelson B R 1974 *Nuclear Structure,* vol 2*, Nuclear Deformations* (New York: Benjamin)
[44] Deubler H H and Dietrich K 1977 *Nucl. Phys.* A **277** 493
[45] Eyal Y *et al* 1980 *Phys. Rev.* C **21** 1377
[46] Aritomo Y, Ohta M, Materna T, Hanappe F and Stuttge L 2004 *Tours Symposium on Nucl. Phys. V, AIP Conf. Proc.* **704** 147
[47] Itkis M G 2004 private communication